Article

Comparison of the Contrail Drift Parameters Calculated Based on the Radiosonde Observation and ERA5 Reanalysis Data

Ilia Bryukhanov *[ID], Oleg Loktyushin, Evgeny Ni, Ignatii Samokhvalov, Konstantin Pustovalov [ID] and Olesia Kuchinskaia

National Research Tomsk State University, 634050 Tomsk, Russia; lega.lega123@mail.ru (O.L.); niev@mail.tsu.ru (E.N.); lidar@mail.tsu.ru (I.S.); k.n.pustovalov@mail.tsu.ru (K.P.); olesia.kuchinskaia@cern.ch (O.K.)
* Correspondence: plyton@mail.tsu.ru; Tel.: +7-952-882-41-94

Abstract: Aircraft contrails exhibit optical properties similar to those of natural high-level clouds (HLCs) and also form persistent cirrus cloudiness. This paper outlines a methodology for detecting and identifying contrails based on the joint analysis of aircraft trajectories (ADS-B monitoring), the vertical profiles of meteorological parameters (radiosonde observation (RAOB) and ERA5 reanalysis), and polarization laser sensing data obtained with the matrix polarization lidar. The potential application of ERA5 reanalysis for determining contrail drift parameters (azimuth, speed, distance, duration, and time of the contrail appearance above the lidar) and interpreting atmospheric polarization laser sensing data in terms of the presence of crystalline ice particles and the assessment of the degree of their horizontal orientation is demonstrated. In the examined case (6 February 2023; Boeing 777-F contrail; flight altitude of 10.3 km; HLC altitude range registered with the lidar of 9.5–10.3 km), the difference in the times of appearance of the contrail over the lidar, calculated from RAOB and ERA5 data, did not exceed 10 min. The difference in the wind direction was 12°, with a wind speed difference of 2 m/s, and the drift distance was approximately the same at about 30 km. The demonstrated technique will allow the experimental dataset of contrail optical and microphysical characteristics to be enhanced and empirical relationships between these characteristics and meteorological quantities to be established.

Keywords: high-level clouds; contrails; polarization lidar; backscattering phase matrix; vertical and temporal profiles of meteorological quantities; radiosonde observations; ERA5 reanalysis

1. Introduction

Climate change is becoming more noticeable, and therefore it is urgent to create and develop empirical models that improve the accuracy of weather and climate forecasting. This problem requires a deeper understanding of atmospheric processes and phenomena. Scientists from various countries predict that the duration of seasons will change [1], ocean currents will cool [2], the Arctic will be almost completely free of ice [3], and even aircraft flights will be limited due to loss of wing lift force with increasing air temperature [4]. Nevertheless, atmospheric models used for weather and climate prediction still fail to provide the required accuracy, primarily due to the limited understanding of certain atmospheric phenomena and processes. High-level clouds (HLCs) are known for their significant contribution to weather and climate processes due to their extensive horizontal extent (up to thousands of kilometers). To assess the HLC effect on radiation, including shortwave solar radiation, it is crucial to know the parameters of their microstructure: size, shape, and spatial orientation of ice particles in them. Under certain conditions, these particles have a predominant horizontal orientation leading to anomalous (specular) backscattering [5–8]. As with natural atmospheric HLCs, the contrail microstructure is not considered in existing atmospheric models, leading to inaccuracies in weather and climate forecasts.

Aircraft contrails possess optical characteristics comparable to those of natural high-level clouds. They reduce solar radiation fluxes and trigger the formation and expansion of cirrus clouds. High-level clouds formed from contrails contribute to anthropogenic climate change. The lifetime of such clouds is determined by meteorological conditions. The World Meteorological Organization has classified contrails lasting longer than 10 min as the sole artificial variety of ice clouds [9]. The appearance of contrails behind aircraft was observed at the beginning of the 20th century. In 1926, Peppler observed a bright halo in the contrail formed at an altitude of 10 km at a temperature of $-50\,°C$, which indicated its crystalline structure [10]. Weickmann [11], who directly studied the contrail microstructure, showed that for about the first 100 m, contrails consist of droplets and then of crystals. Studies of the effect of aviation on atmospheric processes were initiated in the early 1970s by the first estimates of the possible impact of supersonic passenger aircraft flights on the ozone layer [12,13].

Observations of HLCs in northern latitudes from 1975 to 1994 revealed [14] a rise in their formation frequency as aviation activity increased. Measuring contrail properties is challenging because contact instruments on aircraft provide limited data (for example, information about the orientation of ice particles is lost during sampling), and contrails at the initial formation stage are indistinguishable from space platforms due to their small transverse dimensions. Contrails become detectable by satellite instruments 1–2 h after an aircraft passes, which is less than ideal given that their typical lifespan ranges from 1 to 6 h [15].

The task of detecting contrails with satellite instruments is hampered by contrails' low optical density; small width, which exceeds the resolution of the instruments; and low contrast with the background, especially in the presence of clouds or an inhomogeneous surface. Expanding over time, contrails become less dense and difficult to distinguish even at high instrument resolution. For example, at a resolution of 2 km, only 46% of contrails can be detected under ideal conditions [16]. An analysis [17] of contrails over Western Europe showed their effect on the atmosphere: they cool it during the day and heat it at night. The research was performed using data from SEVIRI, AVHRR, and VIIRS satellite instruments. The authors emphasized that to improve atmospheric models, it is necessary to refine cloud parameters, such as the optical thickness and size of ice crystals. According to MODIS and GOES-13 satellite data, clouds formed from contrails have an optical thickness of two to three times greater than the contrails themselves [18]. In addition, they increase the coverage area by 2.4–7.6 times affecting the radiation budget of the atmosphere.

Unlike contact instruments, polarization lidar enables the remote assessment of cloud microstructure parameters, including the orientation of the ice particles within them without disturbing them. Since 2009, the National Research Tomsk State University (NR TSU) has performed regular atmospheric studies using its high-altitude matrix polarization lidar (HAMPL) system for laser polarization sensing experiments [16]. The most reliable source of vertical profiles of meteorological quantities is RAOB. The weather stations closest to the HAMPL location point (Kolpashevo and Novosibirsk) launch radiosondes only twice a day and are more than 200 km away from Tomsk. ERA5 reanalysis, developed at the European Centre for Medium-Range Weather Forecasts (ECMWF), provides high spatial (about 28×28 km) and temporal (1 h) resolutions.

In the present article, we investigated the possibility of using the vertical profiles of meteorological quantities from ERA5 reanalysis data to calculate the parameters of contrail drift based on the comparison with those calculated based on radiosonde observation data. The use of ERA5 data can potentially improve the accuracy of identifying contrails in lidar measurements and obtain information about their optical, geometric, and microphysical characteristics. The purpose of this work is to test this possibility.

2. Materials and Methods

Lidars (including ground-based ones) are the most promising option for solving the problems of operational control and the monitoring of the atmospheric state, since they

allow the vertical profiles of the optical, microphysical, and meteorological characteristics of the atmosphere to be determined in real time. Since the polarization of optical radiation is sensitive to the microstructure of the scattering medium, monitoring its changes in lidar measurements allows the microphysical properties of clouds to be studied.

2.1. High-Altitude Matrix Polarization Lidar Developed at the National Research Tomsk State University

NR TSU HAMPL implements a full cycle of polarization measurements required to obtain all elements of the backscattering phase matrices (BSPMs) of the examined clouds [16–19]. This characteristic mathematically describes the change in the polarization state of optical radiation when it interacts with the scattering volume, and physically contains the information about its microstructure. The block diagram of the lidar is shown in Figure 1.
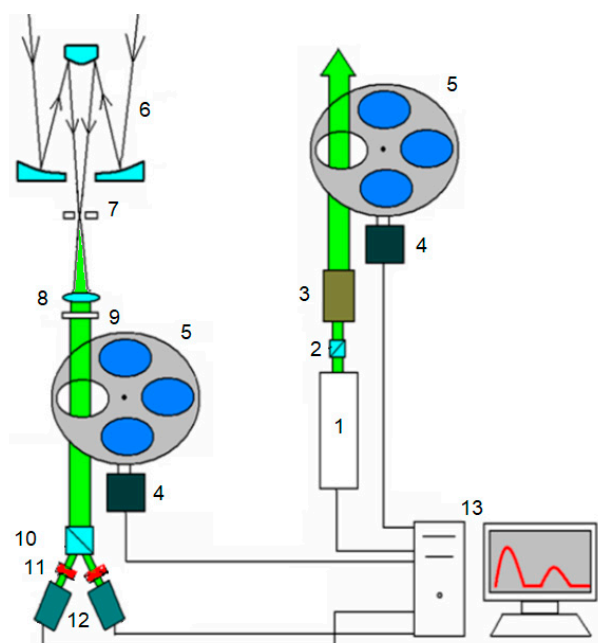

Figure 1. HAMPL system layout includes the following components: 1—laser source; 2—Glan–Taylor prism; 3—lens collimator; 4—stepper motor unit; 5—polarization control unit; 6—Cassegrain mirror telescope; 7—aperture stop; 8—converging lens; 9—interference filter; 10—Wollaston prism; 11—photomultiplier tubes; 12—electro-optic shutters; 13—computerized equipment for data acquisition and visualization [20].

The high-altitude matrix polarization lidar, positioned in Tomsk, operates vertically, aligned with the zenith. A LOTIS TII Nd:YAG laser is used as the sensing radiation source, featuring a wavelength of 532 nm, a 10 Hz pulse repetition rate, and pulse energy reaching up to 400 mJ. Radiation passes through a Glan prism, a collimator (reducing the beam divergence), and a polarization state transformation unit, after which it is sent into the atmosphere in a direction close to the zenith. The receiving antenna uses a Cassegrain telescope with a main mirror diameter of 0.5 m and a focal length of 5 m. An aperture stop, which determines the field of view of the receiving system, is installed in its focal plane; then a collecting lens, the front focus of which is combined with the rear focus of the lens is mounted. After passing through the lens, the beam of received radiation becomes quasi-parallel and passes through an interference filter, a polarization unit, and a Wollaston prism, forming two beams with mutually orthogonal polarizations. They are sent to the Hamamatsu H5783P photonic multipliers operating in photon counting mode, the signal of which is digitized by a two-channel photon counter manufactured by Becker & Hickl GmbH. To reduce the error in estimating the lidar signal, 100–500 sensing

pulses are accumulated during each time period, corresponding to a spatial resolution of 37.5–150 m [20].

The use of the polarization units in the lidar transmitting and receiving systems allows radiation with four polarization states to be sent into the atmosphere alternately and the Stokes vector parameter of backscattered radiation to be determined. This ensures that the experiment obtains all 16 BSPM elements. Coupled with the strobing of the lidar signal, the described technical solution is aimed at obtaining BSPM vertical profiles. In addition, based on the analysis of the vertical intensity profile of the lidar signal for the empty windows of the polarization units in the transmitting and receiving lidar systems, the altitudes of the lower and upper HLC boundaries are determined, as well as the HLC scattering ratio (the ratio of the sum of the coefficients of molecular and aerosol backscattering to the first of these coefficients) and optical thickness (the integral of the attenuation coefficient).

Several regular civil aviation routes are located within a radius of 250 km around the HAMPL point. This allows the study of contrails through polarization lidar to be performed under favorable conditions (wind direction at the flight altitude ensuring drift to the lidar; lack of precipitation and low clouds). Some results of such works have been published previously (for example, in [21]).

2.2. Contrail Identification

Information about the air traffic situation is available in real time through ADS-B (Automatic Dependent Surveillance-Broadcast) monitoring (for example, [22]). The trajectory of each aircraft is represented by a set of points for which coordinates, altitude, date, and time are provided. Depending on the altitude of the aircraft flight, the corresponding wind direction and speed are determined from vertical profiles of meteorological parameters obtained from weather stations located in Kolpashevo and Novosibirsk (Figure 2).
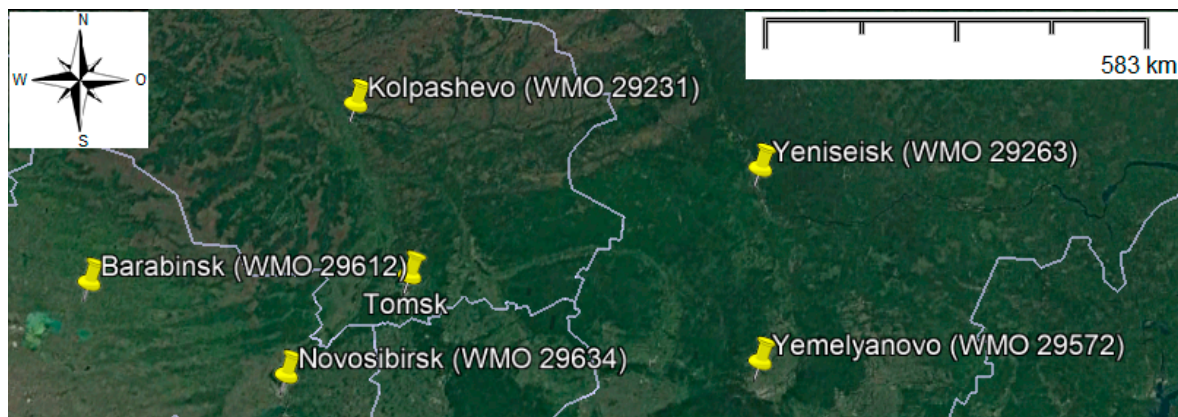

Figure 2. Weather stations within a radius of 500 km from Tomsk [20].

A fragment of a typical aircraft flight trajectory near the HAMPL location point is shown in Figure 3 (the map was obtained using the Google Earth geographic information system). The azimuth from the lidar (*L*) location to the point (*T*) of the aircraft flight trajectory point (this direction corresponds to the meteorological wind direction) was calculated using the following formula [23]:

$$\theta_{LT} = \operatorname{a} \tan 2\left(\frac{\sin(Lng_L - Lng_T) \cdot \cos(Lat_L)}{\cos(Lat_T) \cdot \sin(Lat_L) - \sin(Lat_T) \cdot \cos(Lat_L) \cdot \cos(Lng_L - Lng_T)}\right). \quad (1)$$

If the calculated azimuth corresponds to the wind direction at the flight altitude, then the distance to the lidar coordinate point is calculated for the given trajectory point [23]:

$$d_{TL} = R \cdot \arccos(\sin(Lat_T) \cdot \sin(Lat_L) + \cos(Lat_T) \cdot \cos(Lat_L) \cdot \cos(Lng_T - Lng_L)), \quad (2)$$

where R is the average radius of the Earth, Lat_T and Lng_T are the latitude and longitude of the trajectory point, and Lat_L and Lng_L are the latitude and longitude of the HAMPL location point. If, during this time, a contrail is observed within the lidar field of view at the altitude of the aircraft flight trajectory used in the calculations, it is identified as the aircraft contrail. It is assumed that meteorological conditions remain constant throughout the entire drift path of the contrail.
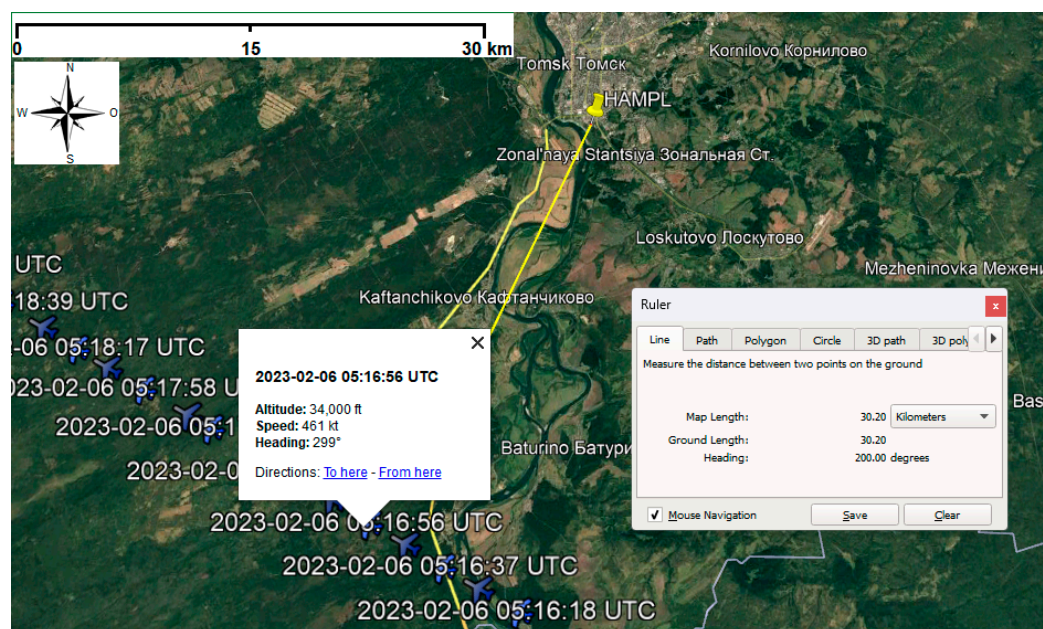

Figure 3. Fragment of the aircraft flight trajectory [22] near the NR TSU HAMPL location.

Previously, the results of radiosonde measurements were used for the described calculations [24] as the most reliable source of meteorological data. The weather stations closest to Tomsk, where such launches are performed, are in Kolpashevo and Novosibirsk (about 240 and 250 km from the HAMPL point, respectively). The locations of these stations, together with the HAMPL location, are shown in Figure 2 (the map was obtained using the Google Earth geographic information system). According to their data, the meteorological situations at the HLC formation altitudes are usually similar, and data on this can be used to assess the atmospheric state above Tomsk. At the same time, discrepancies between the data from simultaneous measurements of the aforementioned stations are not uncommon. In addition, measurements are taken there only twice a day. Thus, the problem of selecting a data source for the vertical profiles of meteorological quantities directly of Tomsk with a higher time resolution is relevant.

ERA5 reanalysis was considered the source of such data [25]. It encompasses a continuous series of meteorological data from 1979 to the present day. The foundational data for ERA5 consist of measurement results collected globally (satellite radiometers; meteorological stations on land, aboard ships, and in aircraft; moored buoys, radiosondes, and ground-based radars) [26]. The time series of air temperature and its derivatives in the reanalysis of the ERA family are consistent for the Siberian region, making them suitable for identifying spatial heterogeneity caused by local factors [27]. ERA5 reanalysis is a popular tool widely used for atmospheric physics problems in various regions of the Earth, as well as in research on the global scale (for example, [28–30]). An assessment of the applicability of such data for the interpretation of data from polarization lidar studies of HLCs in western Siberia [20] highlighted the possibilities of using ERA5.

3. Results

The purpose of the present work is to compare the results of the calculations of the contrail drift parameters (azimuth, speed, distance, duration, and time of the contrail appearance above the lidar) based on ERA5 and RAOB data. These parameters were used to identify and study contrail characteristics according to the data from the HAMPL experiments. Previously [20], based on a 5-year dataset, it was demonstrated that the use of ERA5 data for the HLC formation altitudes in the examined region was correct for a number of meteorological parameters. RAOB data from the weather stations closest to Tomsk and from the time closest to the lidar experiments were used. ERA5 data were selected for the HAMPL coordinates and the time corresponding to the lidar measurements. This article is aimed at demonstrating a methodology for calculating contrail drift parameters. As an example, let us describe measurements on 6 February 2023, during which an aerosol layer was registered at an altitude of about 10.3 km at about 13:00 (local time, Tomsk). It was identified as a contrail of a Boeing 777-F aircraft (flight CZ465/CSN465) [22]. Figure 3 (the map was obtained using the Google Earth geographic information system) shows a fragment of its flight trajectory near Tomsk: at each point of the trajectory, the world coordinated universal time (UTC; Tomsk time is UTC+7 h) is indicated. A straight yellow line on the map connects one of the points of the aircraft flight trajectory with the HAMPL location point. The corresponding azimuth ("Heading") and distance ("Ground Length") are shown in the bottom right corner of the map. The reader should not confuse this with the "Heading" value in the white rectangle on the left side of the figure—this shows the flight course of the aircraft.

Table 1 shows the wind direction and speed based on the RAOB data from the Kolpashevo and Novosibirsk stations. The Kolpashevo station data are missing from the table; apparently, no radiosonde launches were performed there on the considered day. In any case, there are no data from this station available for this day [24]. Note that the wind direction (200°) at the aircraft flight altitude (shown in Figure 2 in the left white rectangle; about 10,363 m) was equal to the azimuth from the HAMPL point to the flight trajectory point, corresponding to 05:16:56 UTC. This leads to the conclusion that the contrail that passed over this point was brought by the wind to the HAMPL point, and thus, it was registered after a time equal to the drift duration.

Table 1. Wind characteristics [24] according to the RAOB data (6 February 2023).

Pressure, hPa	Altitude		Wind Direction, °	Wind Speed, m/s
	ft	m		
Novosibirsk (WMO 29634 station), 00:00 UTC				
250	32,349	9860	190	11
240	**33,172**	**10,111**	**200**	**10**
217	35,200	10,729	215	9
Novosibirsk (WMO 29634 station), 12:00 UTC				
250	32,218	9820	175	13
242	**32,874**	**10,020**	**185**	**12**
200	36,712	11,190	225	11

Table 2 shows similar ERA5 reanalysis data corresponding to the coordinates of the HAMPL point and the aircraft flight date and time for three standard isobaric levels. The second level (highlighted in bold) corresponds to the aircraft flight altitude. By analogy with Table 1, the values in Table 2 closest to the altitude of the considered aircraft flight are highlighted in bold. The wind direction (212°) differs slightly from the RAOB data for the near future and requires the use of another trajectory point to calculate the drift parameters (5:17:26 UTC; the azimuth from the HAMPL point is equal to 212°). The wind speed (10 m/s according to the RAOB from Novosibirsk, 00:00 UTC, versus 8 m/s according to the ERA5 data for Tomsk, 05:00 UTC) varies slightly. The values in pressure and wind

direction and speed shown in the tables are initial integers in the available data. The altitude values are calculated based on reanalysis data for temperature, humidity, and pressure based on a barometric formula and are rounded to integers.

Table 2. Wind characteristics [25] for the NR TSU HAMPL coordinates, according to ERA5 reanalysis data (6 February 2023; 05:00 UTC).

Pressure, hPa	Altitude		Wind Direction, °	Wind Speed, m/s
	ft	m		
250	31,683	9660	209	8
225	**33,757**	**10,289**	**212**	**8**
200	36,093	11,001	233	11

Table 3 presents the characteristics of the specified contrail drift to the HAMPL location point calculated using ERA5 reanalysis and RAOB data. The results of morning measurements were selected as the source of the latter, as they are the closest to the time of the aircraft flight near by the lidar. In this case, data from the Novosibirsk station were used.

Table 3. Characteristics of the contrail drift to the HAMPL location point.

Data Source	Distance, km	Duration (h:mm)	Time (local) of the Contrail Appearance over the HAMPL
Novosibirsk (WMO 29634 station), 00:00 UTC	30	0:51	13:09
ERA5 (Tomsk), 05:00 UTC	30	1:02	13:19

Figure 4 illustrates the dynamics of the vertical profile of the lidar signal intensity at the described time; Figure 5 shows the corresponding profile summed up during a series of measurements (lasting 16 min and 40 s). Note the insignificant discrepancy between the results of the contrail drift parameter calculations using RAOB and ERA5 data not only in drift duration but also in the time of the contrail appearance over the HAMPL.
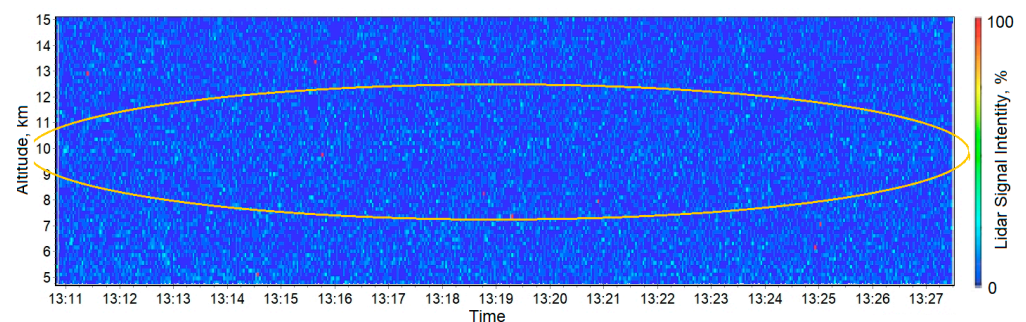

Figure 4. Dynamics of the vertical profile of the lidar signal intensity (6 February 2023; 13:10:49–13:27:31).

In Figure 4, an orange ellipse highlights an increase in the intensity of the lidar signal corresponding to the registration of an aerosol layer. By the time the recording of the considered series of lidar measurements began (at about 13:11 local time; 06:11 UTC), the aerosol layer had already been observed in the field of view of the lidar receiving system; however, it had only recently begun to be observed.
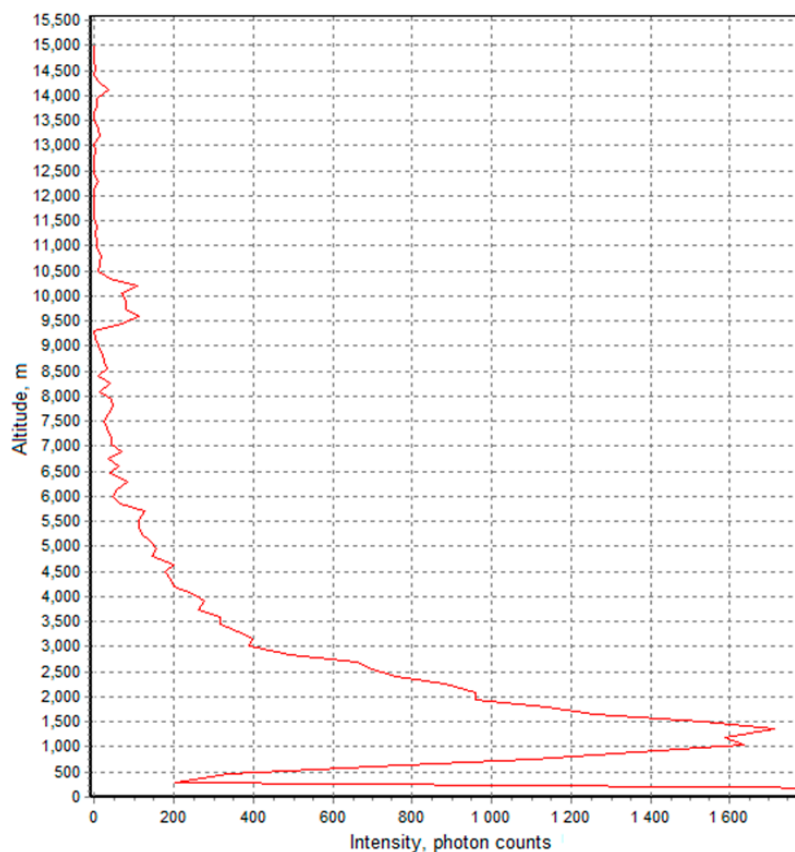
Figure 5. Vertical profile of the lidar signal intensity summed up during a series of measurements on 6 February 2023; 13:10:49–13:27:31).

4. Discussion

The conclusion that the aerosol layer, which was observed at the considered altitude, was a contrail is confirmed by plots in Figures 4 and 5 and by the fact that within a radius of 100 km from Tomsk, civil aviation occurs at two echelons at the following altitudes: 10.2 and 11.4 km [22]. As can be seen from the presented tables and figures, the discrepancies between the results of calculations of the drift parameters of the considered contrail based on RAOB and ERA5 data are not significant. Thus, according to calculations based on both sources of meteorological data, the time of the appearance of the contrail above the HAMPL differs by no more than 10 min, which is less than the duration of one series of lidar measurements (16 min 40 s). Both calculated times fall within the time interval of the same lidar measurement series.

5. Conclusions

An example of the calculation of the contrail drift parameters for its subsequent identification based on the polarization laser sensing data was presented. The obtained discrepancy between the values of the contrail appearance time in the lidar field of view (about 10 min) does not seem significant, even in spite of the 12° difference in wind direction. In the present experiment, the discrepancy in wind speed was only 2 m/s, and the drift distance was approximately equal (about 30 km) for both sources of meteorological data. Thus, it is demonstrated that ERA5 reanalysis can be used to calculate contrail drift parameters.

Based on the obtained results, it can be argued that for the interpretation of the contrail laser sensing data, the ERA5 reanalysis meteorological data calculated directly for the lidar location point and the time closest (with a difference of no more than an hour) to the time of lidar measurements can be used. The described technique will be used to improve the

accuracy of processing the existing array of data from HLC sensing experiments to refine the sample of contrail sensing results. The analysis of such data will allow the study of the optical and microphysical characteristics of contrails, the results of which can be used to improve the accuracy of weather and climate forecasts due to the correct consideration of their microstructures, to be deepened.

Author Contributions: Conceptualization, I.B. and I.S.; software for the lidar, air traffic, and meteorological data processing, visualization, and validation, I.B., O.L., E.N. and I.S.; software for processing the ERA5 data, I.B., E.N. and K.P.; data curation, I.B., I.S., K.P. and O.K. All authors discussed the results and wrote and edited the paper. All authors have read and agreed to the published version of the manuscript.

Institutional Review Board Statement: Not applicable.

Informed Consent Statement: Not applicable.

Data Availability Statement: Publicly available datasets were analyzed in this study. The data can be found here: [http://weather.uwyo.edu (accessed on 11 December 2024)] and [https://cds.climate.copernicus.eu (accessed on 11 December 2024)].

Conflicts of Interest: The authors declare no conflicts of interest.

References

1. Wang, J.; Guan, Y.; Wu, L.; Guan, X.; Cai, W.; Huang, J.; Dong, W.; Zhang, B. Changing lengths of the four seasons by global warming. *Geophys. Res. Lett.* **2021**, *48*, e2020GL091753. [CrossRef]
2. Caesar, L.; Rahmstorf, S.; Robinson, A.; Feulner, G.; Saba, V. Observed fingerprint of a weakening Atlantic Ocean overturning circulation. *Nature* **2018**, *556*, 191–196. [CrossRef] [PubMed]
3. Notz, D.; SIMIP Community. Arctic Sea Ice in CMIP6. *Geophys. Res. Lett.* **2020**, *47*, e2019GL086749. [CrossRef]
4. Coffel, E.D.; Thompson, T.R.; Horton, R.M. The impacts of rising temperatures on aircraft takeoff performance. *Clim. Change* **2017**, *144*, 381–388. [CrossRef]
5. Platt, C.M.R.; Abshire, N.L.; McNice, G.T. Some Microphysical Properties of an Ice Cloud from Lidar Observation of Horizontally Oriented Crystals. *J. Appl. Meteorol. Climatol.* **1978**, *17*, 1220–1224. [CrossRef]
6. Chepfer, H.; Brogniez, G.; Goloub, P.; Bréon, F.M.; Flamant, P.H. Observations of horizontally oriented ice crystals in cirrus clouds with POLDER-1/ADEOS-1. *J. Quant. Spectrosc. Radiat. Transf.* **1999**, *63*, 521–543. [CrossRef]
7. Kaul, B.; Samokhvalov, I.; Volkov, S. Investigating particle orientation in cirrus clouds by measuring backscattering phase matrices with lidar. *Appl. Opt.* **2004**, *43*, 6620–6628. [CrossRef]
8. Kikuchi, M.; Okamoto, H.; Sato, K. A Climatological View of Horizontal Ice Plates in Clouds: Findings From Nadir and Off-Nadir CALIPSO Observations. *JGR Atmos.* **2021**, *126*, e2020JD033562. [CrossRef]
9. Kärcher, B. Formation and Radiative Forcing of Contrail Cirrus. *Nat. Commun.* **2018**, *9*, 1824:1–1824:17. [CrossRef]
10. Peppler, W. Unterkuhlte Wasserwolken und Eiswolken. *Forsch, Erfahr. d, R.W.D.* Reihe B. Nr 1, 1940. (p. 16). Available online: https://www.uwyo.edu/atsc/directory/faculty/emeritus/Vali/ice-init-history.pdf (accessed on 16 October 2024).
11. Weickmann, H. Formen und Bildung atmosphärischer Eiskristalle. *Beiträge Phys. Freien Atmosphäre* **1945**, *28*, 12–52.
12. Johnston, H.S. Reduction of stratospheric ozone by nitrogen oxide catalysis from supersonic transport exhaust. *Science* **1971**, *173*, 517–522. [CrossRef] [PubMed]
13. Crutzen, P.J. Ozone production rates in oxygen, hydrogen, nitrogen oxide atmosphere. *J. Geophys. Res.* **1971**, *76*, 7311–7327. [CrossRef]
14. Minnis, P.; Ayers, J.K.; Palikonda, R.; Phan, D. Contrails, Cirrus Trends, and Climate. *J. Clim.* **2004**, *17*, 1671–1685. [CrossRef]
15. Gierens, K.; Vazquez-Navarro, M. Statistical analysis of contrail lifetimes from a satellite perspective. *Meteorol. Z.* **2018**, *27*, 183–193. [CrossRef]
16. Driver, O.G.A.; Stettler, M.E.J.; Gryspeerdt, E. Factors limiting contrail detection in satellite imagery. *EGUsphere Prepr.* **2024**. [CrossRef]

17. Wang, X.; Wolf, K.; Boucher, O.; Bellouin, N. Radiative effect of two contrail cirrus outbreaks over Western Europe estimated using geostationary satellite observations and radiative transfer calculations. *Geophys. Res. Lett.* **2024**, *51*, e2024GL108452. [CrossRef]
18. Minnis, P.; Bedka, S.T.; Duda, D.P.; Bedka, K.M.; Chee, T.; Ayers, J.K.; Palikonda, R.; Spangenberg, D.A.; Khlopenkov, K.V.; Boeke, R. Linear contrail and contrail cirrus properties determinedfrom satellite data. *Geophys. Res. Lett.* **2013**, *40*, 3220–3226. [CrossRef]
19. Samohvalov, I.V.; Kaul, B.V.; Nasonov, S.V.; Zhivotenyuk, I.V.; Bryukhanov, I.D. Backscattering Light Matrix of Reflecting High-Level Clouds Consisting of Crystal Mostly Horizontally-Oriented Particles. *Atmos. Ocean. Opt.* **2012**, *25*, 403–411. (In Russian)
20. Kuchinskaia, O.; Bryukhanov, I.; Penzin, M.; Ni, E.; Doroshkevich, A.; Kostyukhin, V.; Samokhvalov, I.; Pustovalov, K.; Bordulev, I.; Bryukhanova, V.; et al. ERA5 Reanalysis for the Data Interpretation on Polarization Laser Sensing of High-Level Clouds. *Remote Sens.* **2023**, *15*, 109. [CrossRef]
21. Samokhvalov, I.V.; Bryukhanov, I.D.; Park, S.; Zhivotenyuk, I.V.; Ni, E.V.; Stykon, A.P. Optical Characteristics of Contrails According to Polarization Lidar Sensing Data. In Proceedings of the 24th International Symposium on Atmospheric and Ocean Optics: Atmospheric Physics, Tomsk, Russia, 2–5 July 2018; Matvienko, G.G., Romanovskii, O.A., Eds.; International Society for Optics and Photonics, SPIE: Bellingham, DC, USA, 2018; Volume 10833, pp. 108335J:1–108335J:6.
22. Flightradar24. Live Air Traffic. Available online: https://www.flightradar24.com (accessed on 16 October 2024).
23. Movable Type Ltd. Available online: http://www.movable-type.co.uk (accessed on 2 December 2024).
24. University of Wyoming. Available online: http://weather.uwyo.edu (accessed on 16 October 2024).
25. Copernicus Climate Data Store. Available online: https://cds.climate.copernicus.eu (accessed on 16 October 2024).
26. ECMWF Confluence Wiki. ERA5: Data Documentation. Available online: https://confluence.ecmwf.int/display/CKB/ERA5:+data+documentation#ERA5:datadocumentation-Introduction (accessed on 16 October 2024).
27. Gordov, E.; Schukin, G.G.; Itkin, D.M.; Karavaev, D.M.; Chichikova, E.F. Analysis of Regional Climatic Processes of Siberia:Approach, Data and Some Results. *Vestn. Novosib. Gos. Univ. Inf. Tehnol.* **2011**, *9*, 56–66. (In Russian)
28. Tomshin, O.; Solovyev, V. Synoptic weather patterns during fire spread events in Siberia. *Sci. Total Environ.* **2024**, *921*, 171205. [CrossRef] [PubMed]
29. Wolf, K.; Bellouin, N.; Boucher, O. Distribution and morphology of non-persistent contrail and persistent contrail formation areas in ERA5. *Atmos. Chem. Phys.* **2024**, *24*, 5009–5024. [CrossRef]
30. Matsunaga, W.K.; Sales, E.S.G.; Júnior, G.C.A.; Silva, M.T.; Lacerda, F.F.; de Paiva Lima, E.; dos Santos, C.A.C.; de Brito, J.I.B. Application of ERA5-Land reanalysis data in zoning of climate risk for corn in the state of Bahia—Brazil. *Theor. Appl. Climatol.* **2024**, *155*, 945–963. [CrossRef]